New post-processing method for interpretation of through casing resistivity (TCR) measurements

Chen Qing[1], David Pardo[2], Li Hong-bin[1], Wang Fu-rong[3]

1. College of Electrical and Electronic Engineering, Huazhong University of Science and Technology, Wuhan, China

2. Department of Applied Mathematics, Statistics, and Operational Research at UPV/EHU, and IKERBASQUE, Basque Foundation for Sciences, Bilbao, Spain

3. China University of Geosciences, Wuhan, China

Abstract: We propose a new iterative method for post-processing through casing resistivity (TCR) measurements. This method can be seen as a correction or extension of Kaufman´s theory to more complex scenarios, in which the casing is no longer assumed to be uniform along the axis of the borehole. It can also be seen as a simplified inversion method based on the main physical principles of TCR measurements. To derive our post-processing method, we first use the method of images, which enable us to introduce all key factors involved on TCR measurements, including casing length, casing radius, casing thickness, formation resistivity, location of injected current, and resistivity distribution of formation layers. Then, we design our iterative Post-processing Method by simplifying the complex formulation resulting from using the method of images. Numerical results using goal-oriented *hp*-FEM simulations show that our correction method provides a more accurate approximation to the actual formation resistivity than that predicted by Kaufman´s theory. In addition, the new method is proven to be very efficient and robust, since it is independent of spatial resistivity variations in the formation.

I Introduction

Acquisition of through-casing resistivity (TCR) measurement was first proposed by Alpin in 1939 [1]. He stated that when a casing is excited with currents, the voltage differences on the casing well are highly influenced by the formation resistivity. Thus, formation resistivity could be inferred by measuring the voltage differences. Due to the weak voltage signals below 1 μV obtained in TCR measurements, Alpin´s method was implemented only several decades later, once recent processing and measurement technologies have allowed to measure low voltage signals accurately. The report on the field test of the prototype of the tool (Vail et al., 1995) was another important step towards the development of the technology. During the last two decades, the interest in electrical logging through casing has grown considerably, since resistivity estimations in cased wells is a topic of great importance for the logging industry.

Several studies have been performed concerning TCR measurements. In particular, vertical resolution of the measurement,

effects caused by the cement sheath, casing inhomogeneities, and the finite length of the casing have been studied by Schenkel (1990), Kaufman and Wightman (1993), Schenkel and Morrison (1994), Tabarovsky et al. (1994), Zinger et al. (1994), and Singer et al. (1995 and 1998) [2]-[10].

Based on Kaufman measurement mode, various attempts have been made to build systems for logging formation resistivity in cased boreholes [11]-[12]. Indeed, Kaufman's model and relative analysis method is always seemed as the theoretical basis of TCR measurement technologies. In order to simplify the analysis process of TCR measurements, Kaufman's model assumes an infinite homogeneous casing and formation. However, the practical metal casing has finite length and formation resistivity is not always homogeneous. Thus, Singer found that the computed apparent resistivity of Kaufman's method is not the real formation resistivity [8]. In order to improve the accuracy of the apparent formation resistivity derived from TCR measurements, some more accurate post-processing method is needed.

In this paper, we propose a new post-processing method for TCR measurements that improves the one derived by Kaufmann, specially, when the casing and formation resistivities are not homogeneous. To this end, we first analyze the main differences between Kaufman's computed result and the real formation resistivity. Due to the large number of factors affecting the actual formation resistivity, we derive a simple iterative method that "corrects" Kaufman´s formula in complex-scenarios, and can be used for the accurate derivation of the formation resistivity. In addition, we have developed a numerical method based on a self-adaptive goal oriented *hp*-finite-element method [15][17], which has been successfully applied to simulate TCR measurements, and to analyze the performance of the post-processing method proposed in this work.

II Problem description

Most TCR measurement logging tools are based on the measurement model of Kaufman, where the casing is assumed to be a highly conductive and uniform steel pipe of infinite length, and the formation can be assumed, for some tests, to be a homogeneous medium around the casing. As shown in Fig.1, the current is injected into the casing from electrode A. The leakage current is perpendicular to the casing. The formation apparent resistivity, ρ_a, around point D can be represented as:

$$\rho_a(z) = \frac{U_D}{\Delta i(z)} \quad , \tag{1}$$

where U_D is the potential at electrode D, and $\Delta i(z)$ is the current leakage per meter at a certain depth.

In fact, the computed result (ρ_a) achieved from equation (1) is not the real formation resistivity but the formation

resistance of the horizontal layer with 1 meter thickness. The transfer factor from ρ_a to the real formation resistivity, ρ, depends on the characteristic mechanical parameters of the casing and the distribution of formation layers with different resistivities. In order to decrease the errors, some method is needed to correct Kaufman's results.

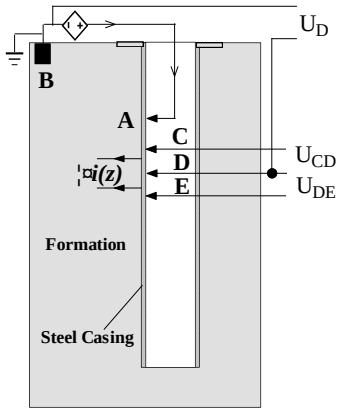

Fig.1 Model of resistivity measurement

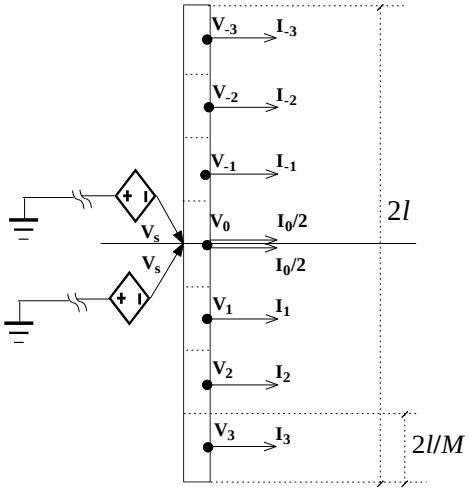

Fig.2 Division of the casing into seven elements

III Theoretical analysis method

On this section we develop a special theoretical analysis based on the method of images, through which the relative potentials and leakage currents are calculated. Since this method generalizes Kaufman's formulas, we can also use it to study the error produced by the latest.

The main objective of the analysis is to determine the potential U_D and the leakage current $\Delta i(z)$ at an arbitrary location on the cylindrical vertical metal casing surrounded by a homogeneous earth, as shown in Fig.1. The casing is taken to have an outer radius a, a thickness Δa, and an overall length l. In carrying out a theoretical direct current (DC) analysis, it is first

assumed that the casing has no longitudinal resistance so the casing can be seemed as an equipotential body. In the next step, the longitudinal resistance of metal casing is included.

The half-space problem can be simplified by using the method of images in which a vertical conductor of twice the original length is embedded into a conductive full space and two in-line voltage sources are installed as shown in Fig.2 [13]-[15]. The double-length casing is divided into M sections (M odd) of length $2l/M$ each. The center point of the outer surface of the nth section will reach a potential V_n, where n ranges from 0 to $\pm(M\text{-}1)/2$. These potentials will have values such that the net current flowing into earth is due to the formation resistivity. The leakage current flowing into earth will be a function of the depth of the section. Because of symmetry, it will be uniformly distributed in the radial direction. In a manner analogous to substitution theory in electrical circuit analysis, the conductor may be removed and replaced by line current sources. The magnitudes of the line current sources are adjusted so that the potential of the casing at the midpoint of the nth section is V_n.

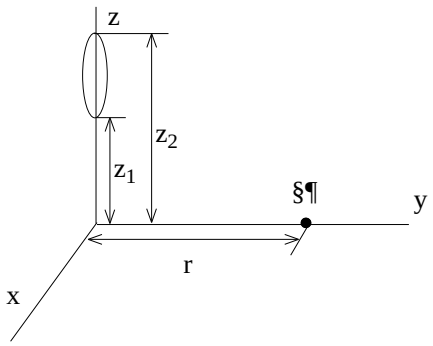

Fig.3 Uniform line current source of total strength *Is* in an infinite earth generating afield point potential. The ellipse represents the source's equipotential surface.

Since the analysis that is used relies heavily on line current source modeling, a line current source embedded into a homogeneous earth is now examined. Consider the situation shown in Fig.3, where a line current source of total intensity I_s is located in an infinitely large homogeneous earth of resistivity ρ. The potential Φ at a field point (x, y, z) with respect to infinity can be calculated by noting that (see [13])

$$\Phi = \frac{I_s \rho}{4\pi(z_2 - z_1)} \ln\left(\frac{z_2 + \sqrt{z_2^{\,2} + r^2}}{z_1 + \sqrt{z_1^{\,2} + r^2}}\right) \tag{2}$$

The quantity Φ/I_s is the transfer resistance between a line current source and a field point. The equipotentials are prolate ellipsoids of revolution that can be used to model elemental sections of the casing, provided the length of the section is large

compared to the radius of the cylinder so that the overlaps at the ends of the section are negligible [14][15].

Suppose the cylinder is replaced by seven (chosen for illustrative purposes) line current sources with voltage sources *Vs* between the double-space casing and infinity, as shown in Fig.2. The potential at the surface of the prolate ellipsoid of revolution that models the elemental cylinder will be given by the summation of the contributions to the potential from all of the elemental line current sources. An initial matrix formulation for a perfectly conducting casing without metal resistance and metal-earth interface resistance can be written by using only the expressions for the self-transfer resistance of elements and the transfer resistance between them.

$$\begin{bmatrix} V_0 \\ V_1 \\ V_2 \\ V_3 \end{bmatrix} = \left[R_+\right] \begin{bmatrix} I_0/2 \\ I_1 \\ I_2 \\ I_3 \end{bmatrix} + \left[R_-\right] \begin{bmatrix} I_0/2 \\ I_{-1} \\ I_{-2} \\ I_{-3} \end{bmatrix} \tag{3}$$

Where

$$\left[R_+\right] = \begin{bmatrix} R_{0,0} & R_{0,1} & R_{0,2} & R_{0,3} \\ R_{1,0} & R_{1,1} & R_{1,2} & R_{1,3} \\ R_{2,0} & R_{2,1} & R_{2,2} & R_{2,3} \\ R_{3,0} & R_{3,1} & R_{3,2} & R_{3,3} \end{bmatrix} \tag{4}$$

$$\left[R_-\right] = \begin{bmatrix} R_{0,0} & R_{0,-1} & R_{0,-2} & R_{0,-3} \\ R_{1,0} & R_{1,-1} & R_{1,-2} & R_{1,-3} \\ R_{2,0} & R_{2,-1} & R_{2,-2} & R_{2,-3} \\ R_{3,0} & R_{3,-1} & R_{3,-2} & R_{3,-3} \end{bmatrix} \tag{5}$$

And

$$\begin{bmatrix} I_0/2 \\ I_1 \\ I_2 \\ I_3 \end{bmatrix} = \begin{bmatrix} I_0/2 \\ I_{-1} \\ I_{-2} \\ I_{-3} \end{bmatrix} \tag{6}$$

Using equation (2), the resistances in equations (4) and (5) can be written as:

$$p = \sqrt{(X-Y)^2}$$

$$R_{X,Y} = \frac{\rho M}{8\pi l} \ln\left(\frac{2p+1+\sqrt{(2p+1)^2+(\frac{Ma}{l})^2}}{2p-1+\sqrt{(2p-1)^2+(\frac{Ma}{l})^2}}\right) \tag{7}$$

In the above formulas, X and Y are integers varying with z_1 and z_2 (X and Y range from 0 to ±3), and ρ is the formation resistivity. Since the casing is assumed to be perfectly conducting in this initial formation, the entire casing settles at a voltage V_s.

$$V_0 = V_1 = V_2 = V_3 = V_s \tag{8}$$

The longitudinal resistance of the cylinder casing can be taken into account as shown in Fig.4. The longitudinal currents between sections are simply related to the individual line current sources I_n. Each longitudinal current labeled in Fig.4 is the average current flowing between the centers of adjacent elements assuming a linearly decreasing flow in each element. When the power supply is located at section 0 (the section closest to the surface of the earth), the potentials of all sections are:

$$\begin{bmatrix} V_0 \\ V_1 \\ V_2 \\ V_3 \end{bmatrix} = \begin{bmatrix} V_s \\ V_s \\ V_s \\ V_s \end{bmatrix} - \gamma_c \begin{bmatrix} 0 & 0 & 0 & 0 \\ \frac{1}{4} & 1 & 2 & \frac{23}{8} \\ 0 & \frac{1}{8} & 1 & \frac{15}{8} \\ 0 & 0 & \frac{1}{8} & \frac{7}{8} \end{bmatrix} \begin{bmatrix} \frac{I_0}{2} \\ I_{-1} \\ I_{-2} \\ I_{-3} \end{bmatrix} \tag{9}$$

In the above formula, γ_c is the casing longitudinal resistance of each section, which can be calculated by using the following equation:

$$\gamma_c = \frac{\rho_c}{\pi(2a-\Delta a)\Delta a}\frac{2l}{M} \tag{10}$$

where ρ_c is the casing resistivity, which is assumed to be $1\times10^{-6}\Omega$m.

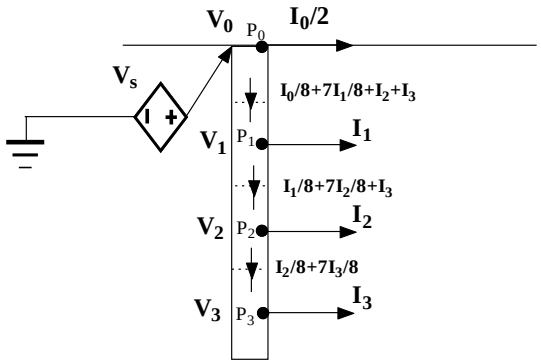

Fig.4. Sectioned casing showing current flowing into the formation and longitudinal current flow.

IV Semi-analytical results

In this section, the factors affecting the difference between Kaufman's result and the real formation resistivity are analyzed one by one through theoretical analysis.

According to the theoretical analysis described above, once the values of l, a, Δa, ρ, ρ_c, and V_s are determined, the leakage currents I_0 to I_M can be determined by equations (3) to (10). Then, the measured formation resistivity can be estimated using equation (2). Fig.5 shows the algorithm to process the solution: the voltage of DC source V_s and the casing resistivity ρ_c are assumed to be 1V and $1\times10^{-6}\Omega$m, respectively. All the analysis results are processed by considering that the double-length casing is divided into seven parts, that is to say, M=7. If higher accuracy is required, the values of M will be increased to 9, 11, or other larger odd number, which will inevitably bring a growth to the computational requirements.

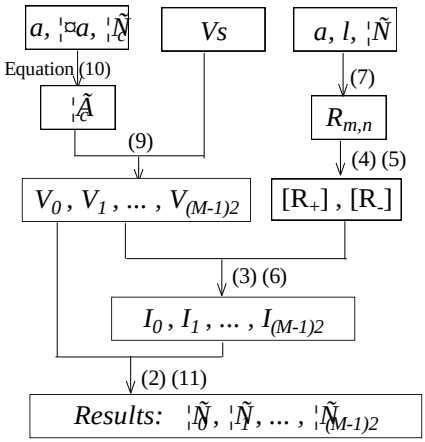

Fig.5. Procedure of computing ρ_a.

The relationship between the total leakage current I_n (n=0,1…,(M-1)/2) and the average leakage current per meter in each section, Δi_n, is described as:

$$\Delta i_n = \frac{M}{2l} I_n \tag{11}$$

Through theoretical analysis, it can be proved that there are differences between Kaufman's computed result and the real formation resistivity. The errors are dependent upon l, a, Δa, ρ, and the current injection point. Here we present some specific examples.

A. Length

A fast personal computer program based on Matlab has been developed to carry out computing tasks. The model casing shown in Fig.1 is divided into seven elements (M=7), and the following values for TCR measurement model are assumed:

$$a = 0.15m;\ \Delta a = 0.01m;\ \rho = 100\Omega m$$

The power supply is located at point '0' as shown in Fig.4. Based on equations (1), (9) and (11), the apparent formation resistivity of section 0 of the casing with different lengths can be easily calculated. Results are shown in Fig.6. Comparing the computed results with the assumed value 100Ωm, we found that the computed results are not the real formation resistivity and the errors are very sensitive to the casing length.

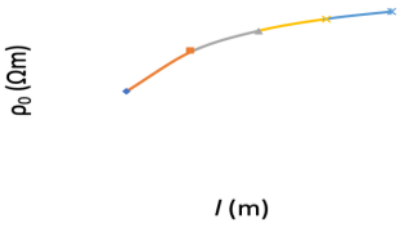

Fig.6. Computed ρ_a for different casing lengths.

B. Radius

We assume the following values for our TCR measurement model:

$$l = 500m;\ \Delta a = 0.01m;\ \rho = 100\Omega m$$

Fig.7 shows the calculated formation resistivity of section 0 of the casing with different radii. The calculated results from Kaufman's theory prove to be strongly dependent upon the casing radius.

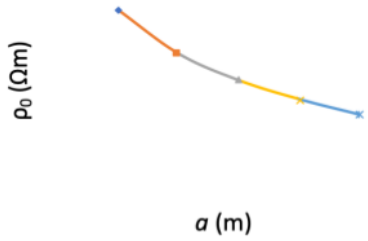

Fig.7. Computed ρ_a for different casing radii.

C. Thickness

Now, we consider the following TCR measurement model:

$$l = 1000m;\ \mathrm{a} = 0.1m;\ \rho = 100\Omega m$$

By modifying the values of Δa, we find whether the calculated results from Kaufman's theory are sensitive to variations of casing thickness. As shown in Fig.8, the computed results grow with increasing Δa, which produces a miscalculation in the apparent longitudinal resistance of the cylinder casing.

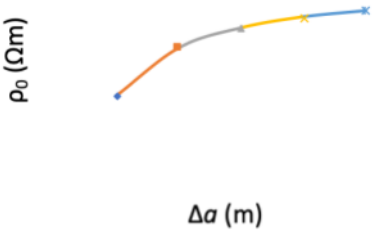

Fig.8. Computed ρ_a for different casing thicknesses.

D. Resistivity

We consider the following TCR measurement model:

$$l = 300m;\ \mathrm{a} = 0.1m;\ \Delta\mathrm{a} = 0.01m$$

Through varying ρ, we find that the difference between results computed according to Kaufman's theory and the real values are also sensitive to the variation of formation resistivity, as shown in Fig.9. It should be noted that the values of vertical axis is the ratio of ρ_0 to ρ.

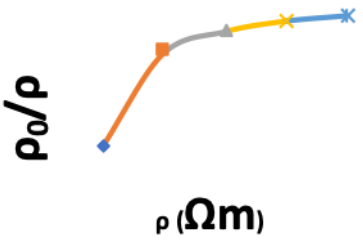

Fig.9. Ratio of ρ_a to real formation resistivity when formation resistivity varies.

E. Location of power supply

In this part, l, a, Δa, and ρ are all set as constants, and the location of power supply is variable.

$$l = 200m;\ a = 0.1m;\ \Delta a = 0.01m;\ \rho = 10\Omega m$$

If the current is injected from section 0, equation (9) describes the relationship among the voltage V_n (n=0,1,2,3),the current I_n, and the supply voltage V_s. Then, the resistivity near section 0 (ρ_0) can be calculated according to the algorithm shown in Fig.5.

If the current is injected from section 1 of casing, the voltage of section 1 will be equal to the supplied voltage V_s, and equation (9) should be modified to be written as:

$$\begin{bmatrix} V_0 \\ V_1 \\ V_2 \\ V_3 \end{bmatrix} = \begin{bmatrix} V_s \\ V_s \\ V_s \\ V_s \end{bmatrix} - \gamma_c \begin{bmatrix} \frac{3}{4} & \frac{1}{8} & 0 & 0 \\ 0 & 0 & 0 & 0 \\ 0 & \frac{1}{8} & \frac{7}{8} & 1 \\ 0 & \frac{1}{8} & 1 & \frac{15}{8} \end{bmatrix} \begin{bmatrix} \frac{I_0}{2} \\ I_{-1} \\ I_{-2} \\ I_{-3} \end{bmatrix} \tag{12}$$

Then, the resistivity near section 1 of casing (ρ_1) will be accurately approximated. Similarly, ρ_2 and ρ_3 can also be calculated. Results shown in TABLE I indicate that location of power supply is another important factor affecting the measurement accuracy of formation resistivity.

TABLE I. Computed ρ_a at different locations.

ρ_0(Ωm)	ρ_1(Ωm)	ρ_2(Ωm)	ρ_3(Ωm)
13.2	13.4	13.1	12.1

V Post-processing Method

Most analytical methods, as the ones shown in Sections III and IV, are useful in analyzing ideal homogeneous

earth-casing model. However, they cannot be applied to complex geometry distributions of formation resistivity. Thus, simulation of TCR measurements via numerical methods becomes rather challenging due to the high electrical conductivity contrast, small thickness of casing and multiplex formation layers [16]-[22]. Here, we employ a numerical method based on a self-adaptive goal oriented *hp*-finite-element method that accurately simulates such logging measurements. The detailed description about the used method of goal oriented *hp*-finite-element simulations can be found in references [16]-[19]. This approach is used to study the behavior of Post-processing Method presented in this paper.

Before introducing our post-processing method, we should study some details on TCR measurement tools. In our specific TCR tool, an electrode-scale consisting of four electrodes (as shown in Fig.11) is used. Electrode A injects DC current, and electrodes C, D, and E are the measuring electrodes, where the potential and second vertical voltage difference can be obtained. We assume the following quantities are known: the electrode potential U_{D_n}, the second vertical voltage difference $\Delta^2 U_n$, the casing length l, the outer radius of casing a, the thickness Δa, and the casing resistivity ρ_c.

In TCR logging, the electrode potentials and second vertical voltage differences are measured, and we can calculate the apparent formation resistivity through Kaufman's method. As analyzed in the previous sections, Kaufman's computed result is not the real formation resistivity, so a special data post-processing method is needed to improve the accuracy of TCR measurements. In the remaining of this section, we describe our post-processing method for TCR measurements. This method is based on an iterative scheme, since otherwise the number of factors and complexity of formulas needed to obtain accurate estimations of the formation resistivity would be too high.

Fig.10 shows the basic steps of our Post-processing Method. Assuming the formation resistivity to be the apparent values from Kaufman's theory, we start our FEM simulations by following the next iterative post-processing method:

1.) The second vertical voltage difference measured at the receiving electrodes is proportional to the leakage of current into the formation as shown in equation (13).

$$\begin{aligned} \Delta^2 U &= (U_C - U_D) - (U_D - U_E) \\ \Delta i &= \frac{\Delta^2 U}{(\Delta z)^2 \gamma_c} = 4\frac{\Delta^2 U}{\gamma_c} \end{aligned} \tag{13}$$

2.) The Kaufman's formation resistivity ρ_n (n=0,1…,(M-1)/2) can be computed via equation (1).

3.) The *hp* FEM simulations can be carried out since the variables ρ_n (n=0,1…,(M-1)/2), l , a , Δa and ρ_c are all known. Then, U'_{D_n} (the new values of potential of electrode D) and $\Delta^2 U'_n$ (the new values of second vertical voltage difference) will be obtained. In order to estimate the accuracy of formation resistivities (ρ_n), the errors, e_n (n=0,1…,(M-1)/2) between

the known values and the new values of potentials and second voltage differences are calculated. Accordingly, the formation resistivities can be corrected from ρ_n to ρ'_n. The values of ρ'_n and e_n (n=0,1…,(M-1)/2) can be easily calculated through equation (14).

$$e_n = \left|\frac{\Delta^2 U'_n - \Delta^2 U_n}{\Delta^2 U_n}\right| * \left|\frac{U'_{D\_n} - U_{D\_n}}{U_{D\_n}}\right|$$
$$\rho'_n = \rho_n \sqrt{U'_{D\_n}\Delta^2 U_n / (U_{D\_n}\Delta^2 U'_n)} \quad (14)$$

4.) If the maximum errors between the known conditions and the new values is below 2%, ρ'_n can be seemed as the actual formation resistivity. Otherwise, the values of ρ_n (n=0,1…,(M-1)/2) will be replaced by those of ρ'_n, and we will iterate the process until we achieve convergence.

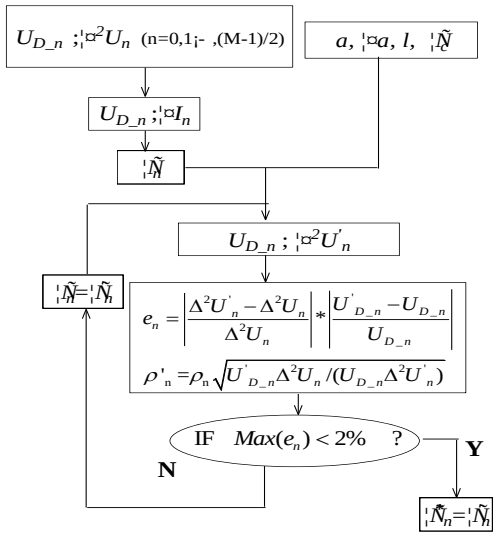

Fig.10. Post-processing algorithm.

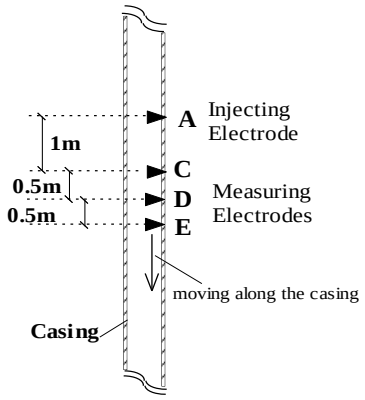

Fig.11. Electrode-scale moving along the casing.

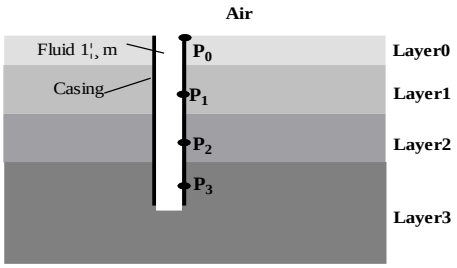

Fig.12 Four formation layers and four current injection electrodes

In order to study the effect of our post-processing method, we will consider two examples.

A. Uniform formation model

As shown in Fig.13, the formation is divided into four layers: (a) Layer 0: 0-30m, (b) Layer 1: 30-90m, (c) Layer2: 90-150m, and (d) Layer 3: 150- ∞ m. The metal casing with a length equal to 210m is consistently divided into four sections: 0-30m; 30-90m; 90-150m; and 150-210m. P_0 is the highest point of casing, and the midpoints of the other three sections of casing are respectively marked as P_1, P_2, and P_3. The outer radius a, the thickness Δa, the injected current, the casing resistivity, and the resistivity of fluid in the borehole are respectively 0.1m, 0.01m, 100A, 0.000001Ωm, and 1Ωm. The four formation layers are assumed to have the same resistivity 10Ωm. Through numerical analysis, we can recover the original formation resistivity.

In order to obtain the formation resistivity of Layer 0, electrode A is located at P_0 and a 100 Amperes current is injected at P_0. Then, the potentials at measuring electrodes C, D, and E can be obtained by numerical simulations. Thus, U_{D_0} and $\Delta^2 U_0$ can be easily calculated through equation (13). The result computed directly from Kaufman's method through equations (1), (10) and (13) is shown in TABLE II, and the calculated value of 13.2Ωm is far away from the real value 10Ωm, since the relative error is over 25%.

In the same way, ρ_1, ρ_2, and ρ_3 (the calculated formation resistivities of Layers 1, 2, and 3) can be easily obtained using Kaufman´s method through equations (1), (10), and (13). All the computed results (respectively 14.7Ωm, 13.9Ωm, and 12.8Ωm) disagree with the real formation resistivity (10Ωm), as shown in TABLE II. Furthermore, the results from simulations meet well with the theoretical analysis results shown in TABLE I, through which the goal-oriented *hp* FEM simulations are proven to have high accuracy.

Then, we continue with our post-processing method by going to step 3 of our algorithm. New values ρ'_n and e_n (n=0,1,2,3) are calculated, as shown in the second row of TABLE III. Since the maximum value of e_n (n=0,1,2,3) is 35%, the values of

ρ_n are replaced by those of ρ'_n and a new simulation is carried out. Through the new simulation, new values of ρ'_n and e_n (n=0,1,2,3) are obtained. As shown in the third row of TABLE III, the maximum value of e_n is 30%, so the iteration procedure continues.

Following the Post-processing algorithm presented above, five iterations are carried out, as shown in TABLE III. The maximum value of e_n decreased gradually, and we finally obtained an error below 2%, as expected. The output resistivity values corresponding to the four layers are respectively 9.9Ωm, 10.1Ωm, 10.1Ωm and 10Ωm, which are all close to the real values.

TABLE II. Original data of uniform model

Injection Point	U_{D_n} (V)	Δ^2U (μV)	ρ_a (Ωm)
P0	7.81	24.8	13.2
P1	7.12	20.3	14.7
P2	6.97	21.0	13.9
P3	7.32	23.9	12.8

TABLE III. Iteration procedure for uniform model

No. of iteration	ρ_0(Ωm)	ρ_1(Ωm)	ρ_2(Ωm)	ρ_3(Ωm)	Max(e_n)
0	13.2	14.7	13.9	12.8	
1	11.3	12.6	11.9	11.3	0.35
2	10.2	10.9	10.8	10.7	0.30
3	9.9	10.5	10.2	10.3	0.10
4	9.8	10.3	10	10.1	0.04
5	9.9	10.1	10.1	10	0.01

TABLE IV. Original data of non-uniform model

Injection Point	U_{D_n} (V)	Δ^2U (μV)	ρ_a (Ωm)
P0	24.6	807	1.28
P1	22.3	236	3.96
P2	25.3	170	6.23
P3	31.2	162	8.07

TABLE V. Iteration procedure for non-uniform model

No. of iteration	ρ_0(Ωm)	ρ_1(Ωm)	ρ_2(Ωm)	ρ_3(Ωm)	Max(e_n)
0	1.28	3.96	6.23	8.07	
1	1.11	3.39	5.54	7.43	0.36
2	1.05	3.18	5.20	7.13	0.13
3	1.02	3.09	5.08	7	0.05
4	1.01	3.03	5.01	7.01	0.01

B. Non-uniform formation model

Now, we consider four formation layers with different resistivities: (a) Layer 0: 1Ωm, (b) Layer 1: 3Ωm, (c) Layer 2: 5Ωm, and (d) Layer 3: 7Ωm. The original data is shown in TABLE IV. The results calculated directly from Kaufman's method are far away from the real formation resistivities. After using the post-processing method, the final corrected results are respectively 1.01Ωm, 3.03Ωm, 5.01Ωm and 7.01Ωm, which are all close to the assumed values, as shown in TABLE V.

VI Conclusion

With the high development of measurement technologies and numerical analysis, interest in electrical logging through casing has grown considerably. Kaufman's theory is always seemed as the basis of through casing resistivity measurement, but the result computed directly from Kaufman's method is not the real formation resistivity but the formation resistance of the horizontal layer with 1 meter thickness.

Through theoretical analysis, the key factors affecting the errors of Kaufman's computed results were found one by one: casing length, casing radius, casing thickness, formation resistivity, location of injected current, and resistivity distribution of formation layers.

By using goal-oriented *hp* FEM simulations with high accuracy, we presented an innovative iteration post-processing method. Assuming the formation resistivities to be the apparent values from Kaufman's method, we start the FEM simulations. Then, we compute new values of potentials and second vertical voltage differences. If the new values from the simulations are close to the known conditions, the apparent formation resistivity is correct. Otherwise, we will carry out more iterative simulations. It is proven that the final output data of iterative simulations are always close to the real formation resistivity distribution, no matter the formation is uniform or non-uniform.

Acknowledgments

The second author was partially supported under the project of the Ministry of Sciences and Innovation MTM2010-16511.

References:

[1] Alpin, L. M., The method for logging in cased wells. U.S.S.R.patent 56026, 1939.

[2] Schenkel, C. J., and Morrison, H. F., "Effects of well casing on potential-field measurements using downhole current sorces," Geophys. Prosp., vol.38, no.6, pp. 663–686, Apr.1990.

[3] Kaufman, A.A., "The electrical field in the borehole with the casing," Geophysics, vol.55, no.1, pp.29–38, 1990.

[4]Kaufman, A.A et.al, "A transmission-line model for electrical logging through casing," Geophysics, vol.58, no.12, pp.1739–1747, 1993.

[5] Vail, W. B, "Through Casing Resistivity Tool TM to locate bypassed oil," The American Oil & Gas Reporter, vol.38, no.11, pp.70–76, Nov.1995.

[6] Schenkel, C. J., and Morrison, H. F., "Electrical resistivity measurement through metal casing," Geophysics, 59, 1072–1082, 1994.

[7] Tabarovsky, L. A, Through-casing resistivity (TCR): Physics, Resolution and 3-D effects: Presented at the 35th Ann. Logging Symposium,

Soc. Prof.Well Log Analysts, 1994.

[8] Zinger, B. Sh. et. al., Modeling of electrical effects of borehole casing inhomogeneities: 64th Ann. Internat. Mtg., Soc. Expl. Geophys., Expanded Abstracts, 399–402, 1994.

[9] Chen Qing, David Pardo, Li Hong-bin, Wang Fu-rong, and Ye Qi-zheng. Arithmetic Method of Double-Injection-Electrode Model for Resistivity Measurement Through Metal Casing. IEEE Trans. on Geoscience&Remote Sensing , vol.48, no.1, pp. 36-41, Jan.2010.

[10] Singer, B.Sh., Through-casing resistivity: 2-D and 3-D distortions and correction techniques: Presented at 36th Ann. Logging Symposium,Soc. Prof.Well Log Analysts, 1995.

[11] Singer, B.S. and Strack K.M. “New aspects of through-casing resistivity theory,” Geophysics, vol.63, no.1, pp.52–63, Jan.1998.

[12] Sheinmann, S. M., On stabilization of electrical fields in the earth: Pricladnaya Geophyzika, 3, 3–15 (in Russian) , 1947.

[13] Trofimenkoff,F.N., “Characterization of EM downhole to surface communication links,” IEEE Trans. on Geoscience&Remote Sensing. Vol.38, no.6, pp.2539-2548, 2000

[14] J.R.Wait, “Theory of transmission of electromagnetic waves along a drill rod in conducting rock,” IEEE Trans. on Geoscience&Remote Sensing. Vol. GE-17, pp. 21–24, Apr. 1979.

[15] M. Y. Xia and Z. Y. Chen, “Attenuation predictions at extremely low frequencies for measurement-while-drilling electromagnetic telemetry system,” IEEE Trans. Geosci. Remote Sensing, vol. 31, pp. 1222–1228, Nov. 1993.

[15] Pardo, D., “Simulation of multifrequency borehole resistivity measurements through metal casing using a goal-oriented hp finite-element method,” IEEE Trans. on Geoscience&Remote Sensing , vol.44, no.8, pp.2125-2134, Aug.2006

[16] Pardo D. , Torres-Verdin C., Nam MJ., Paszynski M. and Calo VM, “Fourier series expansion in a non-orthogonal system of coordinates for the simulation of 3D alternating current borehole resistivity measurements,” Computer methods in applied mechanics and engineering, vol.197, no.45-48, pp.3836-3849,.2008

[17] Pardo D., Demkowicz L., Torres-Verdin C. and Michler C, “PML Enhanced with a self-adaptive coal-orineted hp-finite element method simulation of through casing borehole resistivity measurements” SIAM Journal on scientific computing, vol.30, no.6, pp.2948-2964, 2007

[18] Pardo D, Garcia-Castillo LE, Demkowicz LF and Torres-Verdin C., “A two-dimensional self-adaptive hp finite element method for the characterization of waveguide discontinuities. Part II: Goal-oriented hp-adaptivity,” Computer methods in applied mechanics and engineering, vol.196, no.49-52, pp.4811-4822, 2007

[19] Pardo D., Calo VM., Torres-Verdin C. and Nam MJ. “Fourier series expansion in a non-orthogonal system of coordinates for the simulation of 3D-DC borehole resistivity measurements,” Computer methods in applied mechanics and engineering, vol.197, no.21-24, pp.1906-1925, 2008

[20] Hongnian Wang, “Simultaneous reconstruction of geometric parameter and resistivity around borehole in horizontally stratified formation from multiarray induction logging data,” IEEE Trans. on Geoscience&Remote Sensing. Vol41, no.1, pp.81-89, 2003

[21] Yik-Kiong Hue ,Teixeira, F.L. “Numerical Mode-Matching Method for Tilted-Coil Antennas in Cylindrically Layered Anisotropic Media With Multiple Horizontal Beds” IEEE Trans. on Geoscience&Remote Sensing. Vol.45, no.8, pp.2451-2462, 2007

[22] Guozhong Gao and Carlos Torres-Verdín, “Efficient Numerical Simulation of Axisymmetric Electromagnetic Induction Measurements

Using a High-Order Generalized Extended Born Approximation," IEEE Trans. on Geoscience&Remote Sensing. Vol.44, no.9, pp.2445-2453, 2006